

# We are IntechOpen, the world's leading publisher of Open Access books Built by scientists, for scientists

6,900

Open access books available

186,000

International authors and editors

200M

Downloads

Our authors are among the

154

Countries delivered to

TOP 1%

most cited scientists

12.2%

Contributors from top 500 universities



WEB OF SCIENCE™

Selection of our books indexed in the Book Citation Index  
in Web of Science™ Core Collection (BKCI)

Interested in publishing with us?  
Contact [book.department@intechopen.com](mailto:book.department@intechopen.com)

Numbers displayed above are based on latest data collected.  
For more information visit [www.intechopen.com](http://www.intechopen.com)



# Reverse Satellite Transionospheric Sounding: Advantages and Prospects

*Igor Ivanov, Olga Maltseva, Vladimir Sotskii,  
Alexandr Tertysnikov and Gennadii Zhbakov*

## Abstract

This chapter includes four sections. The first introduction section provides a brief review of the existing methods of transionospheric sounding and the results obtained, and the shortcomings of each are noted. The second section describes the proposed principle based on the installation of a receiver on the GLONASS platform. The advantages and technical characteristics of the proposed system are justified. The main area of use is the polar region. The third section presents the most modern modeling methods and models used. To calculate the propagation of radio waves, this is a method of ray tracing taking into account the large- and small-scale inhomogeneities of the ionosphere. To describe the state of the ionosphere, it is proposed to use the IRI2016 model, which includes adaptation to the current diagnostic data provided by ground ionosondes, and the IRI-Plas model, which not only can be adapted to ground ionosonde data, but also to values of the total electronic content, the measurement of which is an additional advantage of the proposed system. The fourth section includes areas of application, the main of which is the monitoring of the polar region, and the least provided with ionospheric information.

**Keywords:** satellite, satellite information, transionospheric sounding, modeling, radio wave propagation

## 1. Introduction: a brief review of existing methods of transionospheric sounding

The role of the ionosphere in providing human life is difficult to overestimate. This role was great in the pre-satellite era and multiplied after the launch of an artificial Earth satellite. This role is most fully represented in [1], in which various technological systems are divided into two categories: (1) systems which cannot exist without the ionosphere (VLF-LF communication and navigation, MF communication, HF communication, “short-wave” listening, OTH radar surveillance, HFDF and HF SIGINT), and systems on which the ionosphere makes the big impact (a satellite communication, satellite navigation (i.e., GPS & GLONASS, etc.), space-based radar and imaging, terrestrial radar surveillance and tracking, and others). This shows how it is important to study the ionosphere. Classical methods of studying the ionosphere from the Earth’s surface are the pulsed sounding—the sending of radio pulses and the observation of their reflections from various ionospheric

layers with the measurement of the delay time and the study of the intensity and shape of the reflected signals. Measuring the reflection height of radio pulses at different frequencies, determining the critical frequencies of different regions, that is, frequencies for which the given area of the ionosphere becomes transparent, it is possible to determine the value of the electron density in the layers and the virtual altitudes for the given frequencies, hence to select the optimum frequencies for the specified radio paths. This is the principle of work of the main device namely of ionosonde. Its use for many years in many parts of the globe has made it possible to obtain a huge array of data and develop predictive models of various parameters. The breakthrough occurred with the advent of satellites, in particular, with the installation of ionosondes on satellites [2]. Here, there is a wide variety of methods. Let us list some of them with a brief description. The first is external (topside) sounding (TS,  $f < f_oF_2$ , where  $f_oF_2$  is the critical frequency of the basic layer of the ionosphere F2). An example is the on-board ionosonde "IS-338," in future projects, the on-board ionosonde "LAERT" [3]. The second is direct transionospheric sounding (TIS) ( $f > f_oF_2$ ). In this case, the signal is emitted from the spacecraft, and the reception is on the Earth. The third option is reverse transionospheric sounding (RTS) ( $f > f_oF_2$ ). In this case, the signals emitted by the transmitter from the Earth are received by the receiver on the satellite. All of these methods were implemented in a variety of experiments on spacecraft series Alouette, Arial, ISIS, Intercosmos-19 and Kosmos-1809, IC Bulgaria 1300, and others. An example of ionograms of TS (the left curve) and RTS (the right curve) of "Kosmos-1809" is shown in **Figure 1**.

A detailed analysis of the current state of the TS method is given in [4]. The RTS method is presented in [5]. In all cases, a number of important tasks were solved. One of them is the mathematical support of methods [6]. The second problem is the synchronization of airborne and ground ionosondes [7]. **Figure 2** shows a system for synchronous ionospheric sounding using all methods of radio pulse sounding. The features of synchronous operation of the terrestrial-satellite system are presented in the examples of synchronization schemes for previously launched Russian ionosondes.

As to scientific results, it is difficult to select something from hundreds of, if not from thousands of, the publications based on processing of millions of ionograms. As examples, it is possible to note the first publications [8] and the detailed review of results from Alouette1, Explorer 20, Alouette2, Explorer 31 [9]. Data of topside sounding have played a big role in improvement of various models of the ionosphere with the use of data of Intercosmos-19 and Cosmos 1809 [10], Alouette1-2, ISIS-1-2 [11] and later satellites [12]. In the paper [13], application of ionospheric

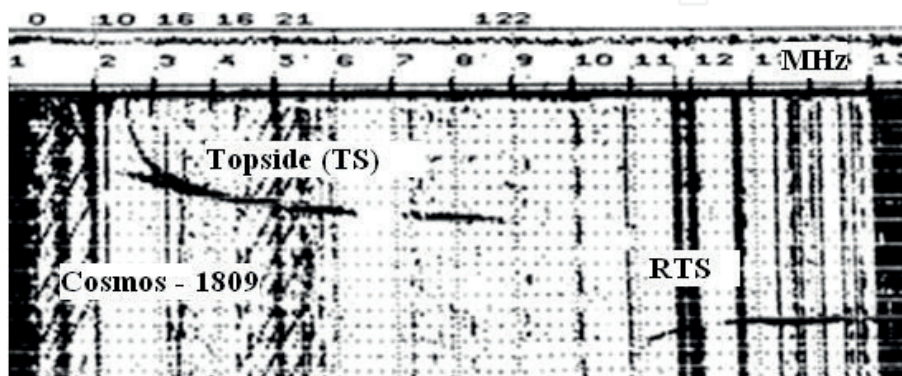


**Figure 1.**  
Example of ionograms of TS and RTS sounding.

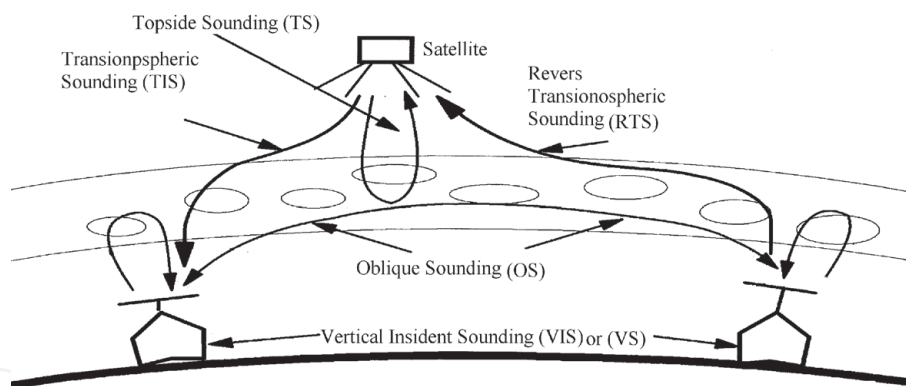


**Figure 2.**  
 Scheme of system sounding of the ionosphere.

topside-sounding results to magnetospheric physics and astrophysics is presented. From the latest publications, it is possible to specify the study of behavior of high-latitude  $N(h)$ -profiles during strong magnetic storms with use of huge database of digital topside ionograms [14]. It is underlined in [4] that the interest in the modification and the use of TIS has increased recently in connection with the need to monitor the polar region. On the one hand, this is due to the fact that high-latitude regions were always problematic zones because of the small number of ionosondes and the enormous spatial and temporal variability of the ionosphere due to the magnetospheric influence. On the other hand, interest increased due to increased scientific and economic activities in these regions.

In this chapter, the main emphasis is also on the study of the polar region, that is why we consider the existing proposals. In [15], the authors, noting such shortcomings of the TIS method, using low-altitude satellites, associated with the high speed of the satellite and its projection to the Earth's surface, as impossibility of exact separation of the spatiotemporal characteristics of the variability in a diagnosed region and large time delay between the measurements of the ionospheric parameters and the processing and analysis of the measurement data, have proposed the use of satellites in the geostationary orbit. Since it is proposed to install a transmitter on a satellite, the main attention in [15] is given to the energy problem. A calculation of ray trajectories is carried out in a two-dimensional plane of propagation from a satellite to a receiver point formed by combined vertical profiles of the electron density. Up to a height of 2000 km,  $N_e(h)$  is taken from the IRI model and then is "sewed" to the NeQuick model [16] in such a way that the electron density becomes zero at a height of 36,000 km. Calculations were made for the transmitting antennas as weakly directed vertical or horizontal dipoles. Of the three types of signals: simple smooth pulses, linearly frequency modulated (LFM) and phase and code manipulated (PCM) used for sounding the ionosphere, estimates are made for the first and second types for signal-to-noise ratio (S/N) of 20 dB. For the first type, the field strength at the receiver was  $\sim 6 \mu\text{B/m}$  for radiated power of 1 kW. The use of LFM signals of  $\sim 100 \mu\text{s}$  duration is intended to reduce the radiated power due to the complexity and broadband of the signals. At  $S/N = 20 \text{ dB}$ , the radiated power can be 100 W. An example of the model transionogram and the received field strength is shown in **Figure 3**.

The paper [17] is a definite addition to [15], of which deserves an attention remark about another disadvantage of this method TIS and RTS, namely, that these techniques only determine two parameters: the critical frequency ( $f_oF_2$ ) and the height of the maximum of the F2 layer ( $h_mF_2$ ) in the sub-satellite point, without defining  $N(h)$ -profile, and that to date conducted only one successful



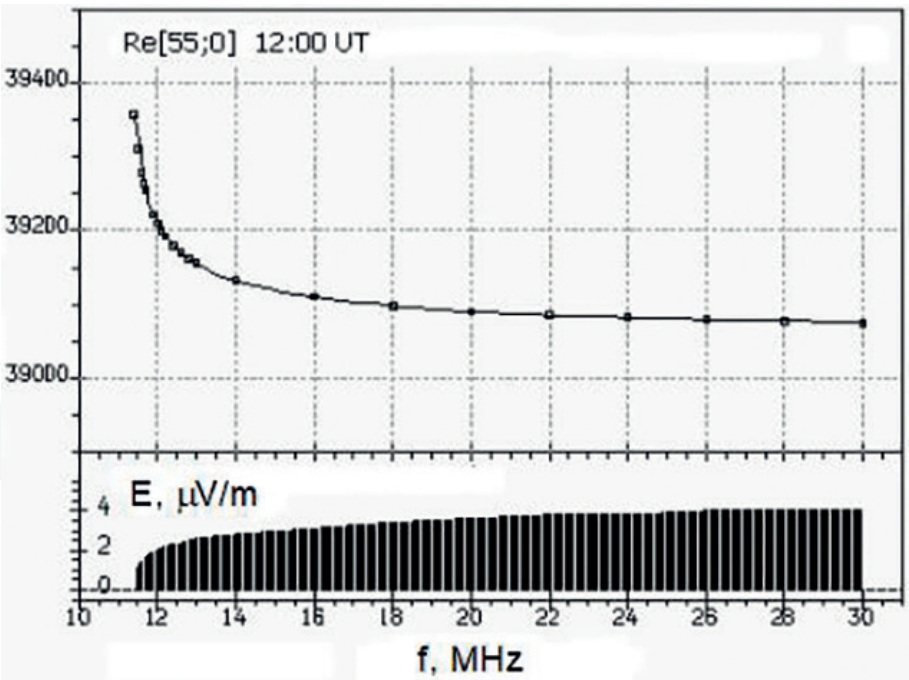


**Figure 3.**  
*Illustration of the sounding method from a geostationary satellite at the point of reception 55° N during the daytime (UT = 12).*

experiment about reconstruction of a bottom Ne(h)-profile of the F2 layer using them [18]. It is possible that namely for this reason, the methods of TIS and RTS have not been developed in the world. Explanation was made for differences of the proposed methods of TS, TIS and RTS: (a) a source of information is not a traditional ionogram and ionogram, retaining only radio sounding signals; (b) ionosonde becomes a measuring tool, and the system of a single-board broadband transmitter module (BTM) and a network of ground receiving k modules (GRM) with the tuning frequency tunable synchronously with the on-board BTM. Therefore, the method is called as multifrequency ionospheric radioscropy method. The difference between [17] and [15] is information on experimental data confirming the possibility of implementing the proposed method, but these data are indirect. The approach described in [19] is based on real experiments in the Arctic using external sounding [20]. These experiments revealed a shortcoming of use of circular low orbit, namely the inability to determine the dynamics of the ionospheric irregularities; therefore, the use of space satellites with highly elliptical orbits with an apogee over the North Pole was proposed. However, it was immediately noted the complexity of using such orbits, consisting in the difficulty of choosing the time of ionosonde location over the investigated area. To overcome this difficulty, it is proposed to use solar-synchronous orbits. It is shown that there is a number of such orbits for monitoring Arctic of Russia: the first orbit has an apogee of 40,000 km (the North Pole) and a perigee of 500 km (above the South Pole) during one revolution of 12 h, a second orbit has an apogee of 20,343 km, perigee 485 km, the time of one revolution is 6 h, the third orbit has apogee 11,829 km, perigee 500 km. The choice of the orbit is mainly influenced by the significant energy loss of the probing signal for propagation in free space. For example, the difference in signal power loss from reflection from the Earth between a high-orbit and low-orbit ionosondes can be about 100 dB, and the transmitter power is limited. As a solution, signals with phase-code modulation are selected. Calculation of the sounding parameters has shown that a power of 600 W will not suppress the remaining experiments on the satellite, and at the same time, this power will be enough to assure confident

reception of signals reflected from the ionosphere of the Earth on a high-altitude apogee satellite. All these proposals indicate the relevance and prospects of such methods.

## 2. The proposed principle

The main element of the methods [15, 17, 19] is the installation of an ionosonde on the spacecraft, but as noted in [21], an ionosonde for TS [19] or a powerful on-board transmitter for TIS [22] not yet created. Even more important is the problem of electromagnetic compatibility on board of a satellite. The proposed principle is a kind of RTS and consists of the use of an on-board receiver and a terrestrial transmitter, which makes it possible to increase the energy potential of the sounding channel due to a more powerful ground-based transmitter. The author of [21] showed the possibility of RTS from highly elliptical orbits up to 40,000 km. The details are as follows. It is proposed to use a terrestrial ionosonde of the “Parus” type with a typical rhombic antenna, only an ionosonde receiver with shortened antennas should be installed on board (the upper part of the frequency range is used). For comparison, the calculation is performed for the orbits proposed in [19], and the characteristics of which are given in **Table 1**. The orbital number, apogee and perigee, eccentricity and period of revolution are given.

The possibility of successful sounding of the ionosphere by means of satellites is largely determined by the energy potential of the Pv channel of the satellite-Earth. The parameter Pv is estimated in [19] for TS and in [17] for TIS. To assess Pv, in the case of RTS, ground and airborne antennas are used, the directional patterns and gain factors are shown in **Figures 4** and **5**. The tables, included in the form of frames, give an idea of the quantitative evaluations: Freq—frequency, R—active resistance, jX—reactive resistance, Ga—gain, F/B—ratio of direct radiation and reverse power, and ON—auxiliary symbol.

The characteristics of the assumed on-board receiver and ground transmitter are given in **Table 2**.

The energy potential of Pv with RTS for orbits with a height of 10–40,000 km was calculated according to the known relation from [23]. The results are shown in **Figure 6**. The red line presents the calculation results for the frequency of 5 MHz, green—10 MHz, blue—15 MHz, dark blue—20 MHz.

In the paper [22], the calculation of the power of the communication channel was carried out for TIS in the circumpolar region, and it is shown that “the main source of background noise is the radiation of powerful radio stations on the Earth’s surface.” That is why, for comparison, **Figure 5**, the dashed curve shows the level of interference from a 21-m broadcast transmitter with a power of 50 kW at the altitudes of the satellite. The peculiarity of the on-board ionosonde “Laert” is a two-channel polarization reception, which allows reducing to a minimum the losses from the polarization mismatch. Losses in antenna feeders

Orbital number	Apogee (km) above the North Pole	Perigee (km)	Eccentricity	Circulation period (h)
1	40,000	500	0.74	12
2	20,343	485	0.591	6
3	11,829	500	0.468	4

**Table 1.**  
*Characteristics of the supposed orbits of satellites.*

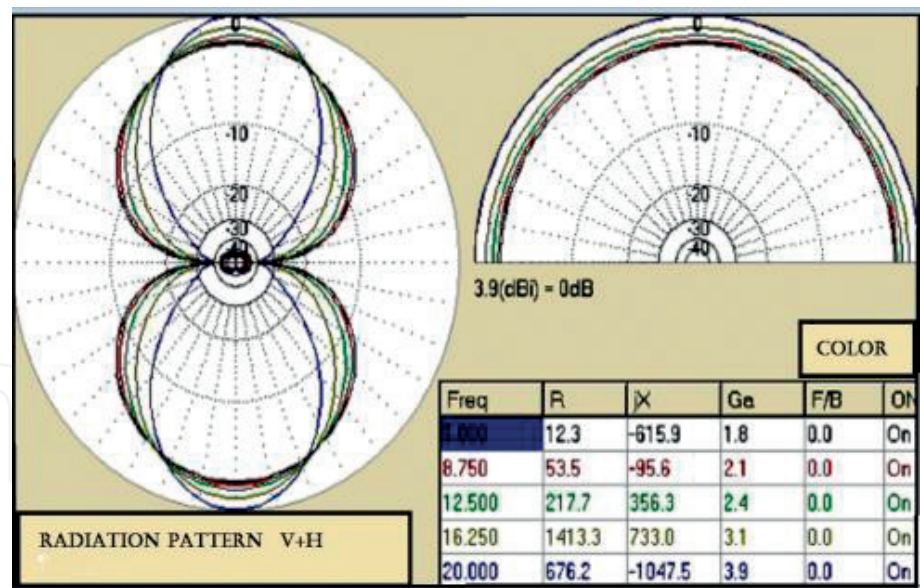


**Figure 4.**  
The calculated radiation patterns and gain factors for on-board orthogonal antennas of 15 m length analogous to the ionosonde antennas of Cosmos-1809.

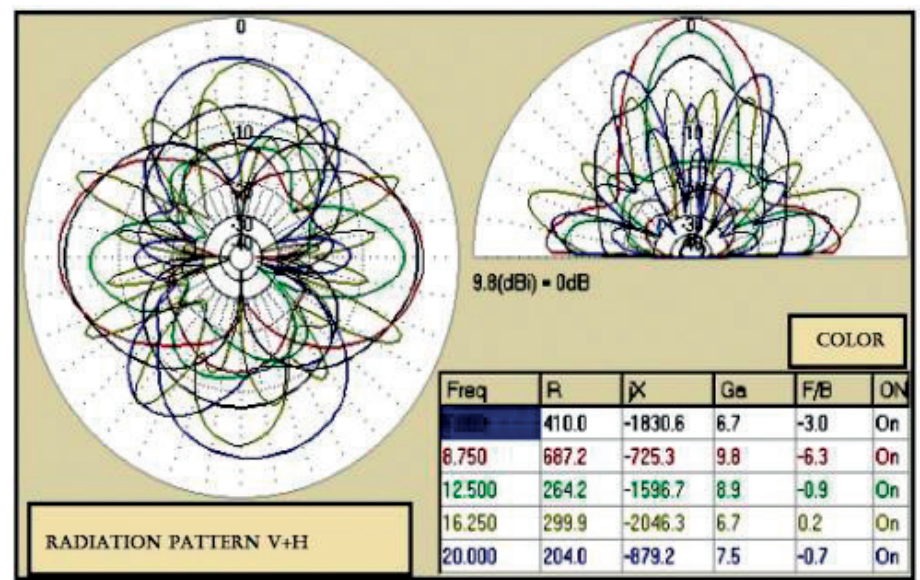


**Figure 5.**  
The directional pattern and the amplification factor of the terrestrial vertical orthorhombic antenna of the VS ionosondes.

and filters are assumed to be 3–6 dB. The obtained values of  $P_v$  show the excess of the signal above the interference to 6–10 dB even for distances exceeding 40,000 km. The worst reception conditions are near the cutoff frequency. In the case under consideration, this frequency of 5 MHz corresponds to  $f_oF_2$ , and it is possible to use a corresponding estimation of absorption. However, in this case too, at a low signal-to-noise ratio (S/N), the transionograms can be recorded, as was shown in the experiments “Intercosmos-19” and RTS—with “Cosmos-1809.” The RTS sounding mode, in which one pulse is emitted at each frequency, ensures maximum diagnostic efficiency, but the “Parus-A” and “Laert” ionosondes are potentially designed to work with complex signals, which can be used to increase the S/N ratio during a significant increase of the absorption in the polar ionosphere during different disturbances. Thus, the RTS mode is energetically favorable for the sounding channel, and it does not require, as with the TIS



Parameter	Receiver of the ionosonde “Laert”	Transmitter ionosonde “Parus-A”	Notes
Range of sounding frequencies (MHz)	0.1–20	0.5–20	Installed programmatically
Pulse power of the transmitter (kW)		Up to 20	Lamp version
Pulse width (μs)	100	20–200	
Pulse repetition frequency (Hz)	60	50–100	Installed programmatically
Bandwidth (kHz)	15		(–3 dB)
Sensitivity (μV)	Not less than 5		With S/N 10 dB
Dynamic range (dB)	Not less than 100		Up to 120
Number of discrete frequencies	400	Not less than 400	Changes programmatically
The law of adjustment in the range	Logarithmic	Linear	Changes programmatically
Instability of reference frequency	Not worse than $10^{-8}$	Not worse than $10^{-8}$	

**Table 2.**  
*Characteristics of prospective receiving and transmitting devices.*

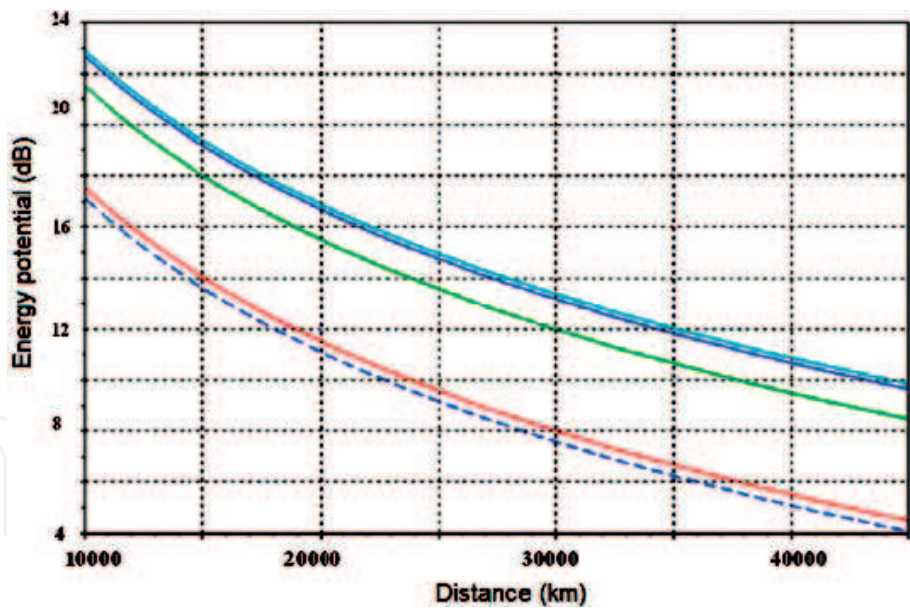


**Figure 6.**  
*The energy potential of the Pv communication channel at the RTS for orbits with a height of 10–40,000 km. Red line shows results for frequency 5 MHz, green—for 10 MHz, blue—for 15 MHz, dark blue—for 20 MHz.*

in [22], to install on the satellite a powerful transmitter that affects the operation of other on-board systems to ensure the requirements of the electromagnetic compatibility. Obviously, working with complex signals, with the accumulation of signals at each sampling frequency [19], significantly reduces the resolution concerning space. The synchronization problem can be solved with the “binding” of the chronographs of the ground and airborne ionosondes to the exact time of GLONASS or GPS [17, 21], taking into account the ephemerides of the satellite.



These results allow us to propose a somewhat different scheme of the RTS method, namely, the use of the GLONASS platform to install the receiver (an application of this method is given in Section 4).

### 3. Used modeling methods and models

#### 3.1 Ionospheric models

Among large number of empirical models of the ionosphere, the International Reference Ionosphere (IRI) is the most widely used, tested by huge scientific community and constantly modified. The development of this model was started in the late 1960s and was carried out under the umbrella of Committee on Space Research COSPAR and International Union of Radio Science URSI. Currently, it is an international standard for the determination of ionospheric parameters [24]. This is a statistical average model based on a huge amount of data from both terrestrial and satellite measurements. For the propagation problems, its most important parameters are: the critical frequency  $f_oF_2$  of the F2 layer (or the maximum density  $N_mF_2$  bound by the linear ratio with the square of the critical frequency), the height  $h_mF_2$  of the maximum of the F2 layer, the propagation coefficient  $M_{3000}F_2$  determining the maximum applicable MUF frequency for the 3000 km path, the altitude profile of the electron density  $N(h)$ , the total electron content TEC of the ionosphere. The parameters are determined using the coefficients of CCIR and URSI, obtained by the Fourier expansion according to the data of the 1960s and the 1980s. The driving parameters are the solar activity indices. The input parameters are the date, latitude and longitude of the point on the globe. The shape of the  $N(h)$ -profile of the lower part of the ionosphere is determined by parameters B0 and B1, for which there are two options: tabular and Gulyaeva data, but they do not have advantages over each other, although the tabular variant is most often used. There are several basic versions of the model, reflecting the most significant stages of its modification: IRI79, IRI90, IRI95, IRI2001, and IRI2007. The latest modifications of the IRI2016 model are presented in [25]. They include two new options for  $h_mF_2$ . The review of the last steps for the transition from climatological character of the model to the description of ionospheric conditions in real time by adaptation to the current diagnostic data is presented. At present, there is a new version of IRI-Plas [26]. The main distinguishing features of this model are: (1) introduction of a new height scale for the upper ionosphere, (2) taking into account the plasma sphere part of the profile and (3) adapting the profile to the experimental value of TEC. The advantages provided by these features are indicated in [27].

#### 3.2 Trajectory calculation method

Like a situation with ionospheric modeling, there is a number of methods of radiowave propagation calculation in the model ionosphere. In this chapter, the most theoretically developed method of trajectory calculations is used. Briefly, it consists of the following. In general, the calculation of trajectories follows the classical ray tracing procedure [28]. A numerical solution of the local dispersion equation is found by transforming it to a system of differential characteristic equations with respect to spatial and ray coordinates in the model ionosphere as the sum of the basic unperturbed part and the additional perturbation:  $N_e = N_0 \cdot (1 + \delta_L + \delta_T)$  where  $N_0$  is the unperturbed “base” part described by the international model IRI-2016, with allowance for the possibility of correction in the presence of experimental vertical sounding data,  $\delta_L$  and  $\delta_T$  are the perturbations created by traveling ionospheric disturbances (TID).

### 3.3 Determination of the parameters of inhomogeneities

Using the proposed method, RTS allows to study in detail not only the large-scale structure in the form of layers, but also to determine the parameters of quasi-wave disturbances, including traveling ionospheric disturbances (TIDs) in the outer ionosphere. The technique was proposed and tested according to the data of RTS on the Intercosmos-1809 satellite. Details of the method are presented in [29]. It is the singular spectrum analysis (SSA) method [30], which is modified to select a one-dimensional latitudinal series of observations of the quasi-harmonic TID component at a fixed height. The investigated series are the values of the electron density at a fixed height in the function of the geomagnetic co-latitude. These series are decomposed into a sum of series, each of which corresponds to a trend, a periodic component and, possibly, noise. The basic algorithm of the SSA method includes four steps: embedding, singular decomposition, grouping, and diagonal averaging. Modification of the basic SSA method consists of removing the trend and analyzing the remaining term characterizing the disturbance. The main contribution is given by decomposition [31]. The method was applied to the case of ionospheric sounding from the Kosmos-1809 satellite on 06.03.1987, pass 1079, UT = 8.82–8.92 h along geomagnetic longitude  $\sim 128^\circ$  E. The geomagnetic situation during the experiment was characterized by the planetary index  $K_p = 2+$ . The spatial distribution of the normalized values of the electron density in the altitude range of 300–400 km is shown in **Figure 7**.

**Figures 8 and 9** show the results of the determination of the electron density perturbation at an altitude of 350 km.

**Figure 8** shows that the disturbance is a fragment of a wave train, not a harmonic. This clearly manifests itself when considering the spatial picture of the disturbance depicted in **Figure 9**. In this particular case, we are dealing with a weak perturbation with a wavelength of  $L \approx 500$  km, damped in the vertical and horizontal directions.

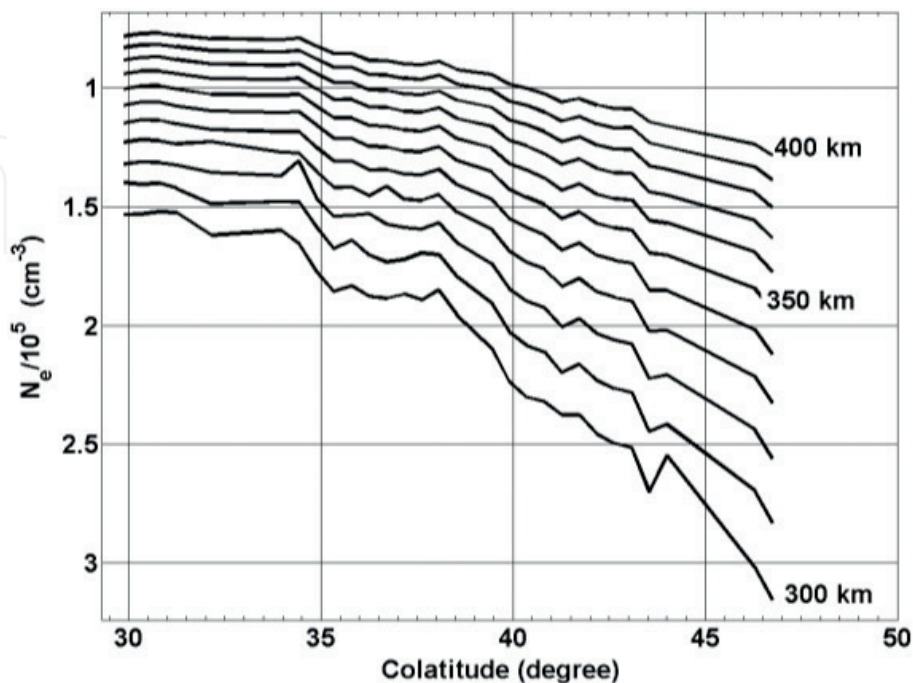


**Figure 7.**  
*Spatial distribution of normalized values of the electron density from topside radio sounding of the ionosphere from the satellite Kosmos-1809.*

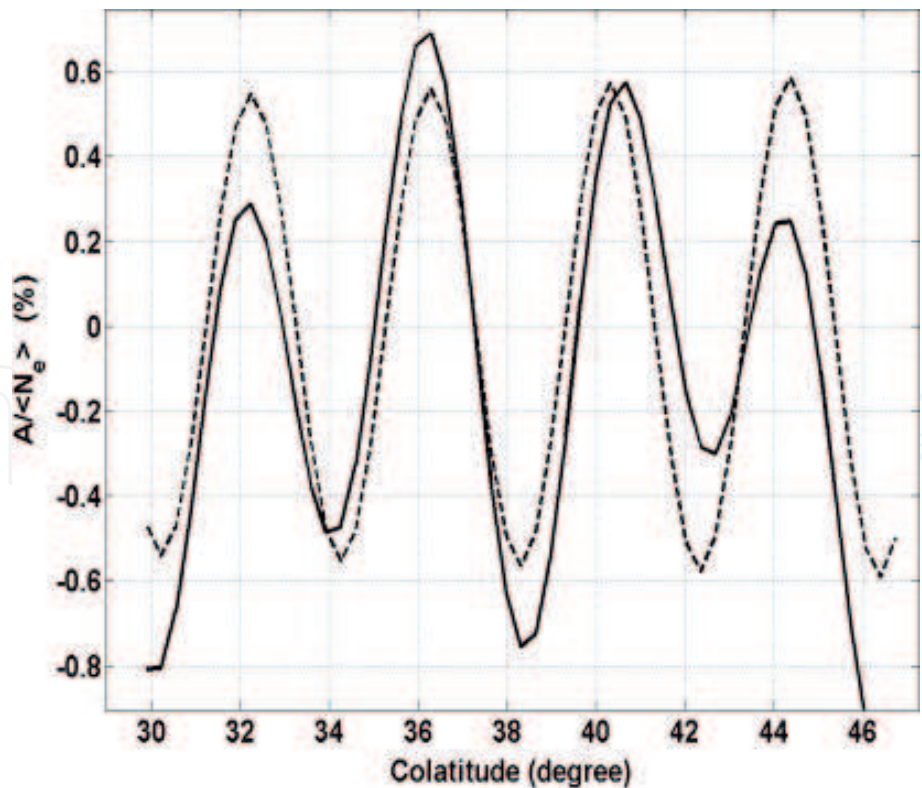


**Figure 8.**  
The results of the analysis of experimental data for the height of 350 km: a quasi-harmonic component of the transformed normalized number (solid line) and its approximation damped sinusoid (dotted line).

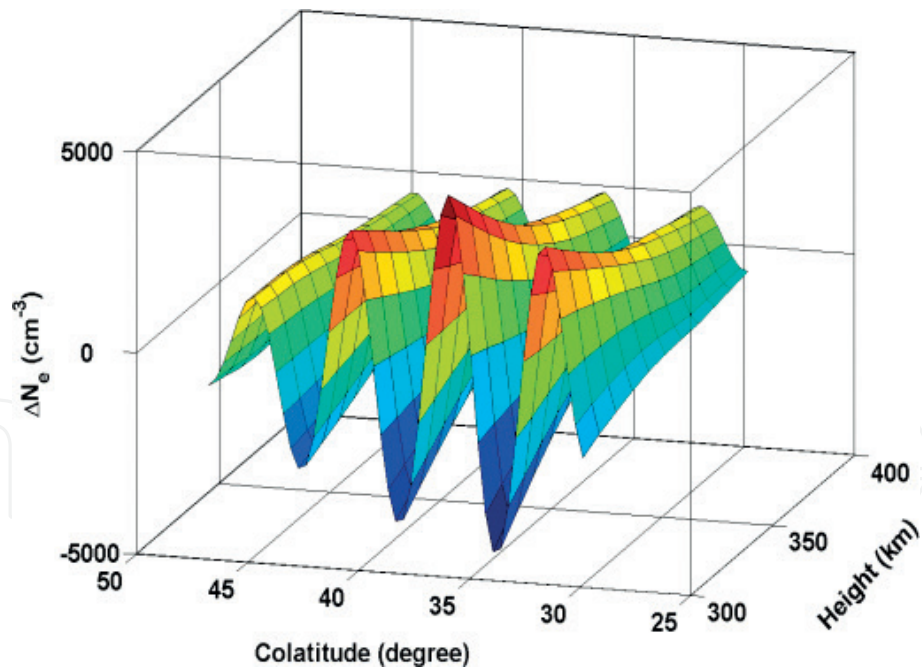


**Figure 9.**  
The spatial pattern of quasi-wave perturbations obtaining in the application of the modified SSA method to the analysis of experimental data of the topside radio sounding ionosphere on board of the satellite “Cosmos-1809” 1987.03.06, at 8.82–8.92 UT.

### 3.4 Use of TEC

TEC measurements by means of signals from satellites began literally with the launch of the first satellite [32]. Since the mid-1960s, continuous measurements of the rotation of the Faraday polarization plane at one point with the help of geostationary satellites have been carried out. Since the mid-1970s, measurements



have been carried out using differential group delays and Doppler shifts. As noted by many researchers, the TEC parameter, like the critical frequency foF2, has become the main parameter for describing the behavior of the ionosphere. A huge number of GPS receivers around the globe, the availability of data on the Internet has allowed and allow scientists to study the local, regional, global characteristics of the ionosphere independently, quickly and simultaneously. The results are presented both on the basis of the data of local networks of GPS receivers, and data of global maps. In this chapter, the TEC values are calculated from the IONEX file data (site <ftp://cddis.gsfc.nasa.gov/pub/gps/products/ionex/>) for the global JPL map.

### 3.5 Examples of using models

Since any empirical model is problematic for the high latitude region, it is necessary to obtain quantitative estimates of the accuracy of the model in the investigated region. In our case, it is the European part of Russia. **Figure 10** gives an example of a comparison of the model and experimental ionospheric parameters for the highest latitude Longyearbuen station (78.2° N, 15.9° E). Its results are compared with the results of the mid-latitude station Juliusruh, which is a reference station. Results are given for mean solar activity from those vertical sounding data that were available for the Longyearbuen station (2011–2014). Absolute  $|\Delta\text{foF2}|$  (in MHz) and relative deviations  $\sigma$  (in %) are compared for three options: (1) model values and experimental medians (“med” icon), (2) model values and monthly average experimental instantaneous values (“ins”), and (3) values calculated using experimental TEC and equivalent slab thickness of the ionosphere  $\tau$  (“ $\tau$ ” icon). The latter should be compared with option 2.

The values averaged over the year during the data availability period of Longyearbuen station are given in **Table 3**. Each result column contains  $|\Delta\text{foF2}|$  and  $\sigma$ . **Figure 9** and **Table 3** show that the average deviations for options 1 and 2 for both stations are not much different. This indicates that the IRI model can provide foF2 with accuracy close to mid-latitude values. Using TEC improves the correspondence between calculated and experimental values in 1.5–2 times; however, here, the results for Longyearbuen station are worse than for Juliusruh. The reason lies in the small number of stations contributing to the construction of global TEC maps, and at large angles of slant TECs associated with the boundary latitude of navigation satellites.

An interesting result was obtained by the author of the model SDMF2 (Satellite and Digisonde Data Model of the F2 layer) for quiet geomagnetic conditions [33] when compared with the IRI model [34]. A comparison was made using data from eight ionosondes in various regions of the globe to evaluate the effects of different solar-ionospheric indices [34]. Of all the stations, the best fit of the model and experimental values of foF2 were obtained for the Salekhard station (66.5°N, 66.5°E).

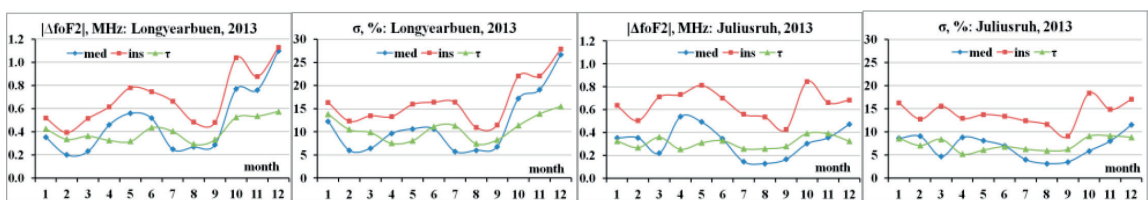


**Figure 10.**  
Comparison of the accuracy of the model for the high-latitude station Longyearbuen and the reference mid-latitude Juliusruh.

	Longyearbuen			Juliusruh		
	med	ins	$\tau$	med	ins	$\tau$
2011	0.42, 11.90	0.64, 17.73	0.38, 11.73	0.44, 10.35	0.65, 14.96	0.28, 6.94
2012	0.36, 9.82	0.62, 17.18	0.43, 12.70	0.76, 17.95	0.99, 23.87	0.38, 9.13
2013	0.48, 11.40	0.69, 16.54	0.40, 10.71	0.32, 6.83	0.65, 13.98	0.31, 7.29
2014	0.70, 13.72	0.85, 17.34	0.42, 9.64	0.62, 11.47	0.83, 15.65	0.30, 6.22

**Table 3.**  
*Comparison of the accuracy of the IRI model from the data of high-latitude and mid-latitude stations.*

The most important is the use of the model to specify propagation conditions on oblique paths. In [35], the calculated and experimental ionograms of oblique sounding were compared on 17 high-latitude HF paths of AARI during the period of quiet conditions on February 13–14, 2014 using the IRI-2012 model. It is shown that the IRI model without correction based on current diagnostic data, even under quiet conditions, underestimates the experimental values. Correction according to the current diagnostic data allows us to substantially approach the calculated values to the experimental ones. As the current diagnostics data, the critical frequencies measured by ionosondes located near the paths or calculated using the experimental values of TEC were used. It was obtained that the relative error of the initial IRI model in obtaining the values of the maximum useable frequency MUF averaged over all cases and the provided 23.6% for one hop was reduced by 4% when using the TEC and by 6% when using foF2. Analysis of experimental data showed that on high-latitude paths, there are a number of unpredictable features that occur even in quiet conditions. These include TID, M and N-modes, lateral modes, triplets and diffusivity. Below, the results of additional comparisons, including for disturbed days on September 6–8, 2017 are presented for ionograms of two oblique paths Cyprus-Lovozero (path length 3600 km) and Gorkovskaya-Lovozero (path length 900 km). It should be noted that the IRI model, like any statistical model, provides median (mean) values, so the model values should be compared with the experimental medians of the parameters. However, very often, model values are used as daily values, that is, instant, for the lack of others. In this case, the error can be large, especially during disturbances. In this case, such disturbance was observed from September 6 to 8, 2017. This fact is illustrated in **Figures 11** and **12**.

For this case, **Table 4** gives mean monthly ( $\Delta$ ), absolute ( $|\Delta|$ ) deviations and estimates of absolute and relative errors.

Relative errors lie in the range of 6–10%. Of course, this is a very small statistic, but it coincides with the results of [36] and allows us to confirm on the new data an important conclusion about the possibility of using the IRI model in high latitudes. **Figure 12** shows the difference in the disturbed values of foF2 from the medians. We see a significant positive disturbance in foF2 on September 7 and a negative perturbation in the behavior of both parameters on September 8. As it was noted earlier, a feature of the IRI model is its ability to be adapted to the current diagnostic data. This plays a big role in the calculation of oblique ionograms, which is illustrated in **Figure 13**. This figure shows the experimental MOF values for one and two hops, as well as the experimental value of foF2 in the center of the path. The black dots show the Dst index reduced in five times in absolute value. The right graph shows the values calculated by the numerical method. Red triangles refer to the experiment, black dots describe the curve for the original IRI model, and blue circles represent the results for model adaptation.

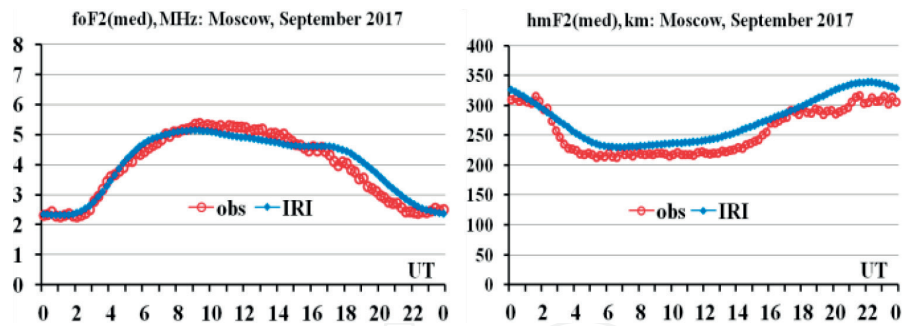


**Figure 11.**  
*Comparison of the model foF2 and hmF2 with experimental medians.*

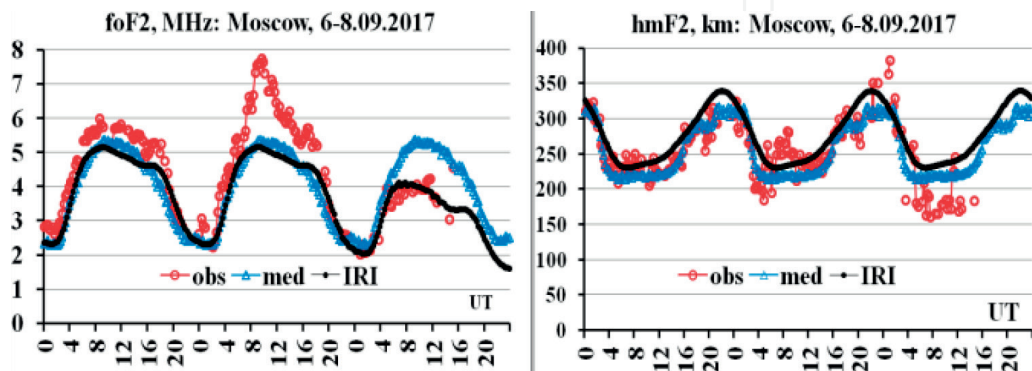


**Figure 12.**  
*Comparison of the model and experimental values of the parameters foF2 and hmF2 during the disturbed period September 6–8, 2017.*

	$\Delta$	$ \Delta $	RMS	RMS (%)
foF2	0.064 MHz	0.22 MHz	0.25 MHz	6.24
hmF2	18.9 km	19.5 km	26.7 km	10.4

**Table 4.**  
*Quantitative estimates of the correspondence between model and experimental medians.*

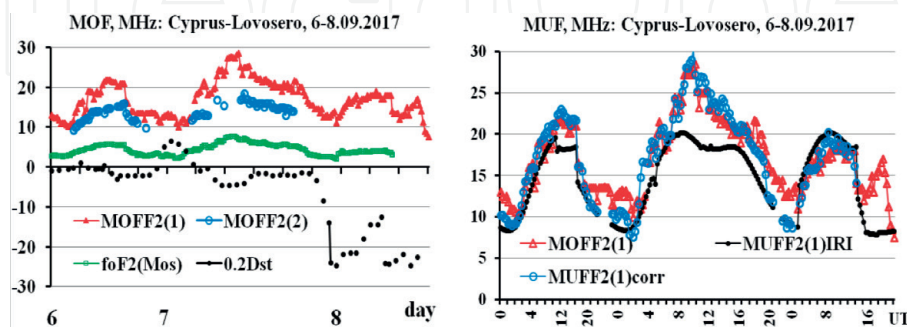


**Figure 13.**  
*Measured and model values of MUF from September 6 to 8 on the path Cyprus-Lovozero.*

This allows us to conclude that the comparison of the parameters of HF propagation testifies that the model can be used in the high latitude region as yet, especially at adaptation to the data of the current diagnostics.



#### 4. Areas of application of the proposed principle

Since the main area of application of the proposed principle is the polar region, it is necessary to point to an important result of [37]. It is shown that when recalculating a slant TEC into a vertical one, the traditional assumption of the ionosphere in the form of a thin layer is admissible. The height of this layer is associated with the position of the sub-ionospheric point. The calculated positions of this point are shown in **Figure 14**. The vertical axis represents the maximum latitude of the sub-ionospheric points in degrees, along the horizontal axis the latitude of the receiver in degrees is postponed.

This indicates that in high latitudes, there is no restriction on the visibility of the satellite, that is, on sounding the high-latitude ionosphere according to GNSS signals, and allows solving such tasks as tracking the position of high-latitude structures: mid latitude ionospheric trough (MIT) and auroral oval. The situation with the study of these structures is as follows. The trough generally consists of three parts: an equator wall, a trough minimum and a pole wall. Because of the large electron density, gradient on either side of the trough affects radio wave propagation, the exact position of the trough is very important for solving some problems, such as trans-ionospheric communication and navigation [38]. The main regularities of the behavior are obtained, and the MIT model is developed using foF2 [12] for night winter conditions—the period of the most probable occurrence of a trough. The corresponding behavior of the TEC shows that TEC can be used to identify the position of the dip [39]. It is shown that TEC always shows the presence of the trough.

The auroral oval in the high-latitude ionosphere is the boundary of the polar cap and is defined as the region of the ionosphere, which is the projection of the plasma layer and cusp along the lines of force of the geomagnetic field. The position of the auroral oval zone is projected onto the boundary of the outer radiation belt of the Earth. During magnetic storms, it shifts toward the mid-latitude, following a shift in the outer radiation belt. The displacement is almost linear and can reach 10 degrees with the growth of the Kp index to 5. With greater growth of Kp, the auroral oval boundary can jump discontinuously in the middle latitudes due to a significant distortion in the structure of the magnetosphere. In the auroral oval zone, the frequency of failures and refusals of radio communication and navigation equipment increases [37], so it is important to monitor its position. The possibility of such tracking not only in the meridional but also in the longitude directions is shown in [40].

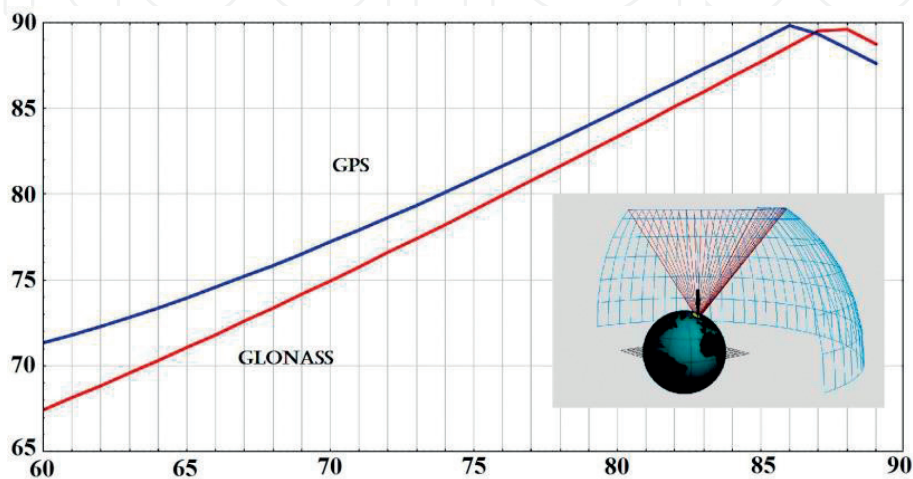


**Figure 14.**  
*Position of the maximum latitude of the sub-ionospheric point, depending on the latitude of the receiver.*

An additional advantage of using the GLONASS platform for implementing the RTS method is associated with the ability to determine the  $N(h)$  profile from the initial height of the ionosphere to the height of the platform. This is due to the possibility of determining the critical frequency that can be used to adapt the model. The simulation results are shown in **Figure 15** for conditions of February 21, 2014, UT = 12, the satellite's altitude is 20,000 km, the satellite's latitude is  $68.96^\circ$ , longitude is  $33.0^\circ$ , the transmitter's latitude is  $68.56^\circ$ , longitude is  $33.08^\circ$ . The left panel of **Figure 15** shows the  $N(h)$ -profile as  $F_n(h)$ -curve ( $N$  is proportional to  $F_n^2$ ), the middle—trajectories of waves, and the right panel shows the transionogram.

It can be seen that foF2 can be determined with an accuracy of 0.25 MHz. In experiments, it is possible to use the basic advantage of the model IRI-Plas, namely, its adaptation to measured value of TEC, which allows modifying plasmaspheric part of  $N(h)$ -profiles.

One more important possible application of the RTS method can be an installation of the receiver on low-flying mini satellites. The launch of such satellites is carried out constantly. It is possible to point out the results presented at the conference [41]. The micro-satellite “Chibis-M” was launched into a near-Earth orbit with parameters close to those of the ISS (513 km altitude, inclination  $51^\circ$ ) on January 25, 2012 as a passing load on the cargo spacecraft Progress. It successfully operated for more than 2.5 years. The Vernov satellite was launched on July 8, 2014 to a solar-synchronous orbit with a small eccentricity—the height of the pericenter is 640 km, the altitude of the apocentre is 830 km, the inclination is  $98.4^\circ$ , and the period of revolution is 100 min. The Lomonosov satellite was launched on April 28, 2016 also to the solar synchronous orbit, circular with a height of 490 km, an inclination of  $98.4^\circ$  and a period of 90 min. The realization of these microsatellites has shown that with their help, it is possible to successfully carry out electromagnetic monitoring of the surrounding space environment. A new space project of the Moscow State University is being discussed (Lomonosov “Universal-SOKRAT”) to create a grouping of satellites for real-time monitoring in near-Earth space. Methodological aspects of the spatiotemporal resolution of the plasma-wave parameters of the ionosphere with the help of two copies of Trabant MC (2020–2024), simultaneously deduced into an orbit with a height of  $\sim 500$  km are considered. They intended for investigation of: (a) the mechanisms of occurrence and dynamics of ionospheric inhomogeneities of different scale depending on the active processes on the Sun and on Earth; (b) regularities of changes in plasma-wave and electromagnetic parameters in the ionosphere of natural and technogenic character in a wide dynamic and frequency ranges; (c) applied aspects, consisting in conducting diagnostics of ionospheric manifestations of space weather.

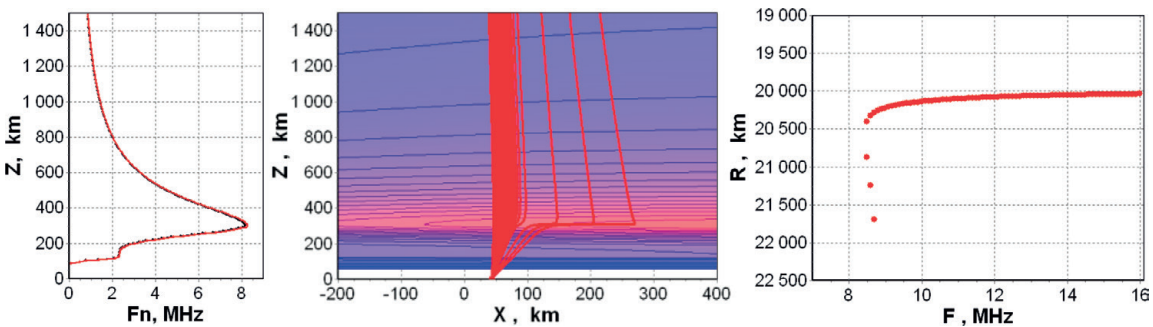


**Figure 15.**  
*Illustration of the possibility to obtain foF2.*

## 5. Conclusions

The long-term use of satellite sounding data has made it possible to obtain the most important knowledge about near-Earth space. Climatological models of ionospheric parameters have been developed, which have found the widest application in various technological systems. However, at the present stage, it is necessary to provide operational support for these systems with ionospheric information. Here, it is necessary to look for ways of modifying different methods. In the ionospheric models, it is an adaptation to the parameters of the current diagnosis and the use of the total electron content for this diagnosis. A modification is also required in transionospheric sounding methods. It is shown that the main role can be played by the method of reverse transionospheric sounding, combined with the measurement of TEC. The installation of an on-board ionosonde receiver on the GLONASS platform helps to solve much problems. First, there is no need to develop a new platform for the polar high-apogee experiment, and second, the installation of the ionosonde receiver does not violate the electromagnetic compatibility requirements, the “timing” of the ionosonde to the exact time and the ephemerides of the satellite is simplified, and the transionograms of the RTS can be transmitted through the service channels, besides, sizes of the reception aerial decrease at restriction of a frequency range [21].

## Acknowledgements

This work was supported by grant under the state task N3.9696.2017/8.9 from Ministry of Education and Science of Russia.

## Conflict of interest

There is no conflict of interest.

## Author details


Igor Ivanov<sup>1</sup>, Olga Maltseva<sup>1\*</sup>, Vladimir Sotskii<sup>1</sup>, Alexandr Tertyshnikov<sup>2</sup> and Gennadii Zhbakov<sup>1</sup>

<sup>1</sup> Institute for Physics, Southern Federal University, Rostov-on-Don, Russia

<sup>2</sup> Institute of Applied Geophysics, Moscow, Russia

\*Address all correspondence to: mai@ip.rsu.ru

## IntechOpen

© 2018 The Author(s). Licensee IntechOpen. This chapter is distributed under the terms of the Creative Commons Attribution License (<http://creativecommons.org/licenses/by/3.0>), which permits unrestricted use, distribution, and reproduction in any medium, provided the original work is properly cited. 



## References

- [1] Goodman JM. Operational communication systems and relationships to the ionosphere and space weather. *Advances in Space Research*. 2005;**36**:2241-2252. DOI: 10.1016/j.asr.2003.05.063
- [2] Florida CD. The development of a series of ionosphere satellites. *Proceedings of the IEEE*. 1969;**57**(6):867-875. DOI: 10.1109/PROC.1969.7132
- [3] Givishvili GV et al. Transionospheric radiosonde based on the onboard ionosonde "LAERT" and ground ionosonde "PARUS-A" (in Russian). *Heliogeophysical Research*. 2015;**12**: 21-28. Available: <http://vestnik.geospace.ru/index.php?id=301>
- [4] Danilkin NP. Transionospheric radiosounding (review). *Geomagnetism and Aeronomy*. 2017;**57**(5):501-511. DOI: 10.1134/S0016793217050048
- [5] Vasiliev GV, Ivanov II, Kovalev SV. Device for the study of the ionosphere. *Certificate of authorship*. USSR № 1. 1986;340-383
- [6] Denisenko PF, Sotskii VV. Specific features of inverse problems of vertical radio sounding of the ionosphere (review). *News of Higher Educational Establishments. North-Caucasian Region*. 1987;**2**:59-71
- [7] Ivanov II. Synchronization of onboard and ground-based ionosondes in systematic sounding of the ionosphere. *Physical Bases of Instrument Making*. 2012;**1**:101-111
- [8] Schmerling ER, Langille RC, guest editors. Special Issue on Topside Sounding and the Ionosphere. In: *Proceedings of the IEEE*. 1969;**57**(6)
- [9] Jackson JE. Results-From-Alouette-1-Explorer-20-Alouette-2-And Explorer-31. July 1988. Available from: <https://ru.scribd.com/document/48695743/Results-From-Alouette-1-Explorer-20-Alouette-2-And-Explorer-31>
- [10] Pulinets SA, Depuev VH, Karpachev AT, Radicella SM, Danilkin NP. Recent advances in topside profile modeling. *Advances in Space Research*. 2002;**29**(6):815-823
- [11] Bilitza D, Reinisch BW, Radicella SM, Pulinets S, Gulyaeva T, Triskova L. Improvements of the international reference ionosphere model for the topside electron density profile. *Radio Science*. 2006;**41**:RS5S15. DOI: 10.1029/2005RS003370
- [12] Karpachev AT, Klimenko MV, Klimenko VV, Pustovalova LV. Empirical model of the main ionospheric trough for the nighttime winter conditions. *The Journal of Atmospheric and Solar-Terrestrial Physics*. 2016;**146**:149-159. DOI: 10.1016/j.jastp.2016.05.008
- [13] Benson RF, Osherovich VA. Application of ionospheric topside-sounding results to magnetospheric physics and astrophysics. *Radio Science*. 2004;**39**:RS1S28. DOI: 10.1029/2002RS002834
- [14] Benson RF, Fainberg J, Osherovich VA, Truhlik V, Wang Y, Bilitza D, Fung SF. High-latitude topside ionospheric vertical electron-density-profile changes in response to large magnetic storms. Available from: <https://ntrs.nasa.gov/search.jsp?R=201600058412018-06-29T13:55:48+00:00Z>
- [15] Givishvili GV, Danilkin NP, Zhabankov GA, Krasheninnikov IV. Possibilities of radio sounding of the ionosphere in the decameter range on board a geostationary satellite. *Geomagnetism and Aeronomy*. 2012;**52**(4):491-496. DOI: 10.1134/S0016793212040032

- [16] Nava B, Coisson P, Radicella SM. A new version of the NeQuick ionosphere electron density model. *The Journal of Atmospheric and Solar-Terrestrial Physics*. 2008;**70**:1856-1862. DOI: 10.1016/j.jastp.2008.01.015
- [17] Givishvili GV. MFRT method—The basis for remote monitoring the ionosphere of the RF polar zone in operative mode. *Heliogeophysical Research*. 2016;**14**:69-81. Available from: <http://vestnik.geospace.ru/index.php?id=435>
- [18] Avdyushin SI, Danilkin NP, Ivanov AI, Ipatov EB, Kushnerevsky YV, Lukin DS, Migulin VV. Transionospheric sounding at the boundary of radio-transparency of the ionosphere. *Geomagnetism and Aeronomy*. 1983;**23**(4):567-572
- [19] Danilkin NP, Zhbankov GA, Zhuravlev SV, Kotonayeva NG, Lapshin VB, Romanov IV. Monitoring of the ionosphere in the Arctic based on satellite ionosondes (in Russian). *Heliogeophysical Research*. 2016;**14**:31-35. Available from: <http://vestnik.geospace.ru/index.php?id=381>
- [20] Danilkin NP, Zhuravlev SV, Kotonayeva NG, Kuraev MA, Anishin MM. Modeling an experiment on radio sounding of the ionosphere from the artificial earth satellite Kosmos 1809 in the presence of vertical electron concentration inhomogeneities in the Arctic region. *Geomagnetism and Aeronomy*. 2012;**52**(2):229-234
- [21] Ivanov II. Ionospheric monitoring in the arctic at reverse transionospheric sounding. In: *Radiation and Scattering of Electromagnetic Waves (RSEMW)*; 26-30 June 2017; Divnomorskoe, Russia. 2017. pp. 118-120. DOI: 10.1109/RSEMW.2017.8103582. Available from: <http://ieeexplore.ieee.org/document/8103582/>
- [22] Krasheninnikov IV. Analysis of the types of probing signals in the problem of ionospheric sounding and criteria for the efficiency of the use of space systems for conducting transionospheric monitoring in the Arctic (in Russian). *Heliogeophysical Research*. 2016;**14**:53-62. Available from: <http://vestnik.geospace.ru/index.php?id=383>
- [23] Tse D, Wiswanath P. *Fundamentals of Wireless Communication*. Cambridge, England: Cambridge University Press; 2005. 564 p
- [24] Gulyaeva TL, Bilitza D. Towards ISO standard Earth ionosphere and plasmasphere model. In: Larsen RJ, editor. *New Developments in the Standard Model*. USA: NOVA Publishers; 2011. pp. 11-64
- [25] Bilitza D, Altadill D, Truhlik V, Shubin V, Galkin I, Reinisch B, Huang X. International reference ionosphere 2016: From ionospheric climate to real-time weather predictions. *Space Weather*. 2017;**15**:418-429. DOI: 10.1002/2016SW001593
- [26] Gulyaeva TL. Storm time behavior of topside scale height inferred from the ionosphere-plasmasphere model driven by the F2 layer peak and GPS-TEC observations. *Advances in Space Research*. 2011;**47**:913-920. DOI: 10.1016/j.asr.2010.10.025
- [27] Maltseva OA, Zhbankov GA, Mozhaeva NS. Advantages of the new model of IRI (IRI-Plas) to study ionospheric environment. *Advances in Radio Science*. 2013;**11**:907-911. DOI: 10.5194/ars-11-307-2013
- [28] Nickisch LJ. Practical applications of Haselgrove's equations for HF systems. *Radio Science Bulletin*. 2008;**325**:36-48. DOI: 10.23919/URSIRSB.2008.7909584
- [29] Denisenko PF, Sotsky VV. Diagnosis of quasi-wave disturbances in near-earth plasma by modified SSA

- method. In: *Radiation and Scattering of Electromagnetic Waves (RSEMW)*; 26-30 June 2017; Divnomorskoe, Russia. 2017. pp. 17-20. DOI: 10.1109/RSEMW.2017.8103550. <http://ieeexplore.ieee.org/document/8103550/>
- [30] Golyandina NE. A Method “Caterpillar”-SSA: The Analysis of Time Rows: The Manual. Stain Petersburg: BBM; 2004. 76 p
- [31] Denisenko PF, Khomyakov AA. Monitoring large-scale moving ionospheric disturbances according to satellite sounding. *Electromagnetic Waves and Electronic Systems*. 2014;**19**(9):22-25
- [32] Aitchison GJ, Weekes K. Some deductions of ionospheric information from the observations of emissions from satellite 1957a2-I. *Journal of Atmospheric and Terrestrial Physics*. 1959;**14**:236-243
- [33] Shubin VN. Global empirical model of critical frequency of the ionospheric F2-layer for quiet geomagnetic conditions. *Geomagnetism and Aeronomy*. 2017;**57**(4):450-462. DOI: 10.1134/S0016793217040181
- [34] Shubin VN. Comparison of solar-ionospheric indices for the foF2 modeling. In: *Proceedings of the 2ndURSI AT-RASC*; 28 May–1 June 2018; Gran Canaria
- [35] Blagoveshchensky DV, Maltseva OA, Anishin MM, Rogov DD, Sergeeva MA. Modeling of HF propagation at high latitudes on the basis of IRI. *Advances in Space Research*. 2016;**57**:821-834. DOI: 10.1016/j.asr.2015.11.029
- [36] Maltseva OA, Mozhaeva NS, Nikitenko TV. Comparison of model and experimental ionospheric parameters in the auroral zone. *Advances in Space Research*. 2013;**51**(4):599-609. DOI: 10.1016/j.asr.2012.04.009
- [37] Kovalev DS, Tertyshnikov AV, Chukin VV, Glukhov YV. Experiments on ionospheric research on board of the arctic floating university. *Scholarly Notes*. 2016;**41**:156-164
- [38] Yang N, Le H, Liu L. Statistical analysis of ionospheric mid-latitude trough over the Northern Hemisphere derived from GPS total electron content data. *Earth, Planets and Space*. 2015;**67**:196. DOI: 10.1186/s40623-015-0365-1
- [39] Maltseva O. Verification of Ionospheric Models by TEC and Satellite Measurements ICTRS'17; November 6-7, 2017; Delft, Netherlands© 2017 Association for Computing Machinery. ACM. ISBN 978-1-4503-6364-8/17/11...\$15.00 <https://doi.org/10.1145/3152808.3152817>
- [40] Tertyshnikov AV. The manifestation of the auroral oval over Antarctica in the characteristics of GNSS signals 17.01.2015 near the station “Vostok”. *Heliogeophysical Research*. 2016;**14**: 31-35. Available from: <http://vestnik.geospace.ru/index.php?id=459>
- [41] Abstracts of 13th annual conference “Physics of plasma in solar system”; February, 12-16th 2018; Moscow, ICR. 383 p